Robust image de-blurring with inaccurate blur kernels

Hui Ji and Kang Wang

Abstract

Most existing non-blind image deblurring methods assume that the blur kernel is free of error. However, it is often unavoidable in practice that the input blur kernel is erroneous to some extent. Sometimes the error could be severe, e.g, for images degraded by non-uniform motion blurring. When an inaccurate blur kernel is used as the input, significant distortions will appear in the image recovered by existing methods. In this paper, we present a novel convex minimization model that explicitly takes account of errors in the blur kernel. The resulting minimization problem can be be efficiently solved by the so-called APG method. Also, a new boundary extension scheme is incorporated in the proposed model to further improve the results. The experiments on both synthesized and real images showed the efficiency and robustness of our algorithm to both the image noise and the model error in blur kernel.

Index Terms

wavelet tight frame, image de-convolution, ℓ_1 norm minimization, accelerated proximal gradient method

EDICS Category

TEC-MRS, TEC-RST

I. INTRODUCTION

Image blurring is one of the prime causes of poor image quality in digital imaging. Two main causes of blurry images are out-of-focus and camera shake. The image blurring process is commonly modeled as the convolution of a clear image with a shift-invariant kernel plus noise:

$$f = k * g + n, \tag{1}$$

where '$*$' denotes the discrete convolution operator, g denotes the clear image, f denotes the available blurry observation, k denotes the blur kernel and n denotes the image noise. Recently, spatially variant blurring models also has drawn a lot of attentions (e.g. [1]–[3]) for better modeling practical motion blurring. Both spatially invariant and spatially varying image blurring processes can be expressed in a matrix-vector form:

$$\mathbf{f} = \mathcal{A}\mathbf{g} + \mathbf{n} \tag{2}$$

where $\mathbf{f}$, $\mathbf{g}$, $\mathbf{n}$ denote the column-wise vector forms of f, g and n respectively, and the matrix $\mathcal{A}$ denotes the blurring matrix. For spatially invariant blurring process, each row of $\mathcal{A}$ corresponds to the same smoothing filter up to a spatial shift. For spatially varying image blurring process, each row of $\mathcal{A}$ may correspond to a different smoothing filter.

Image deblurring is about how to estimate the clear image g from the given blurry image f. There are two tightly coupled sub-problems: (a) estimating the blur kernel k (or $\mathcal{A}$) and (b) estimating the clear image g using the estimated blur kernel k. Existing image deblurring methods can thus be classified into two categories: *blind image deblurring* that jointly solves the above two sub-problems and *non-blind image deblurring* that only solves the second sub-problem. It is well known that the non-blind image deblurring is an ill-conditioned problem in the presence of image noise, as some high-frequency components are attenuated in the blurring process such that they

H. Ji, and K. Wang are with Department of Mathematics, National University of Singapore, Singapore 117543, Singapore (email: matjh, wangkang@nus.edu.sg).

can barely be discriminated from the noise. Simply reversing the blurring process may considerably amplify the noise and do more harm than good. Blind image deblurring is an even more inherently ill-posed problem due to the loss of information on both the images and the blurring process.

In the past, there have been extensive studies on how to improve the robustness of non-blind image deblurring methods to image noise. Most of them assume the blur kernel provided for the image deblurring is free of error. However, in practice, such an assumption often does not hold true. Taking motion deblurring for example, the existing approach for the blur kernel estimation either is done by using some additional hardwares that augment the camera system to aid the blurring process (e.g. [4]–[6]), or is done by using software-based blind motion deblurring techniques that impose certain priors on motion-blur kernels to significantly constrain the form of kernels (e.g. [7]–[10]). Despite the great progresses on blind motion deblurring, there are several issues that limit the wider applicability of these methods. One is due to the complex nature of the practical blurring process, the priors used for constraining kernels may not characterize the real blur kernels very accurately. As a result, the accuracy of the estimated blur kernels varies with different data sets. Another issue is that the convolution model (1) is often over-simplified for many practical motion-blurred images. It is shown in Levin et al. [11] that the uniform blurring assumption on motion blurring caused by camera shake often is an over-simplified assumption. Practical motion blurring tends to be a spatially varying blurring process. Although there have been some interesting work on estimating spatially varying blurring matrix $\mathcal{A}$ (e.g. [1], [3], [12]), how to reliably estimate such a matrix $\mathcal{A}$ without auxiliary hardwares remains an open question.

Without taking account of the error in the blur kernel, non-blind deblurring methods are indeed very sensitive to even a small amount of perturbations on blur kernels. See Fig. 1 for an illustration of the sensitivity of the widely used Richardson-Lucy (RL) method to image noise and kernel error. Clearly, besides the image noise, the sensitivity of the deblurring method to the error in blur kernel k (or in the blurring matrix $\mathcal{A}$) should be addressed when developing practical image deblurring methods. Thus, this paper aims at developing a new non-blind image deblurring method which not only is robust to image noise but also is robust to the blur kernel error or model error in $\mathcal{A}$. In this paper, a new regularization based approach is proposed to solve the following errors-in-variables (EIV) version of (2) :

$$\mathbf{f} = (\mathcal{A} - \delta_{\mathcal{A}})\mathbf{g} + \mathbf{n} \tag{3}$$

where $\delta_{\mathcal{A}}$ is the model error in $\mathcal{A}$ and $\mathbf{n}$ is additive image noise. The proposed minimization is convex and can be efficiently solved by the so-called *accelerated proximal gradient* (APG) method with mathematically guaranteed fast convergence. Also, a new technique of handling boundary value problem is introduced in this paper which outperforms the existing boundary extension techniques, especially when the blurring is significant or spatially variant.

A. Related work

Image deblurring is one long-last problem in image processing. There have been an abundant literature on this topic. The entire body of previous work on this topic is beyond what can be covered here. Thus, we will only discuss some most related non-blind and blind deblurring techniques. The ill-posedness of the image deblurring problem comes from the ill-conditioning of the blurring matrix $\mathcal{A}$ when solving the linear system (2). Early traditional image deblurring methods work in the frequency domain as the convolution operator can be diagonalized by the Fourier transform, e.g., the *wiener filter* based deconvolution ([13]) minimizes the negative impact of noise at frequencies with poor signal-to-noise ratio. Rather than taking inverse filter in the frequency domain, another type of deblurring method is using a Bayesian-based iterative procedure for recovering sharp images. One such representative approach is the so-called Richardson-Lucy (RL) method ([14], [15]) that utilizes the Bayes' law to make the inference about clear image iteratively. The RL method is adapted in [16] to handle spatially varying motion blurring. These methods are very simple to implement and the results are relatively of fine quality. However, unpleasant ringing artifacts near strong edges are known as the side effect of these methods.

In recent years, regularization based methods have been widely used to overcome the ill-conditioning of the matrix $\mathcal{A}$. The estimation of clear image in most regularization methods is done by solving the following minimization:

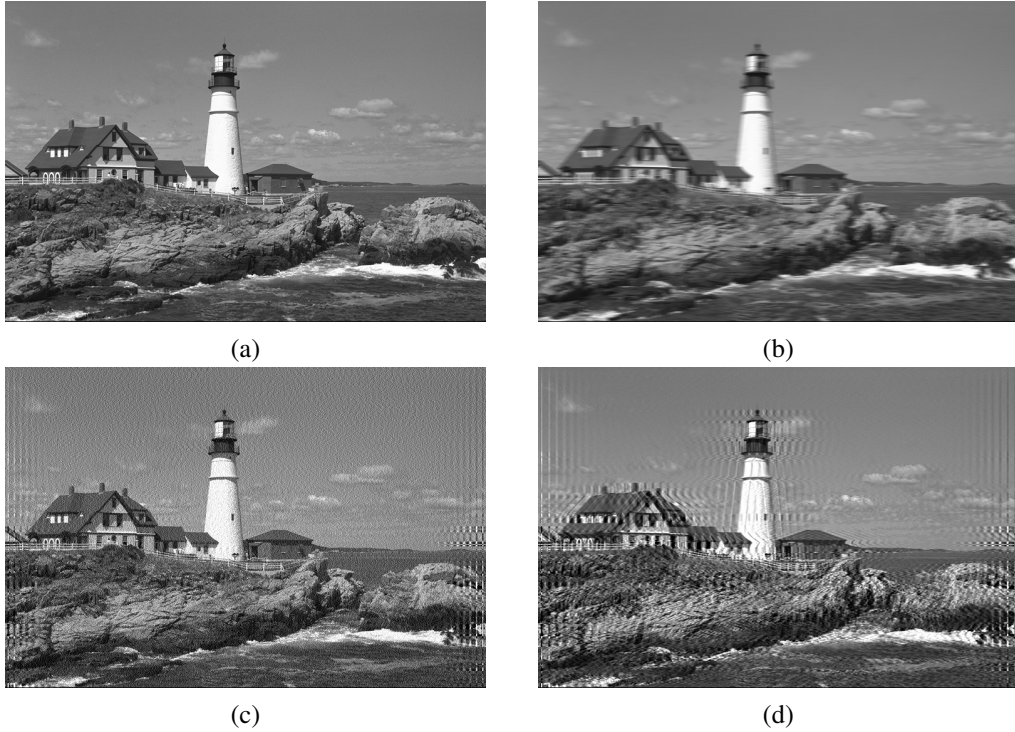$$\min_{g \in \mathbb{R}^n} \Phi(\mathcal{A}\mathbf{g} - \mathbf{f}) + \Psi(\mathbf{g}), \tag{4}$$

Fig. 1. Illustration of the sensitivity of the RL method to kernel error and noise. (a): original image; (b): image blurred by the horizontal linear motion kernel of length 10 pixels; (c): result of the RL method for the blurred image shown in (b) further corrupted by Gaussian white noise with variance $\sigma = 2$; (d): de-blurred result of the RL method for the blurred image shown in (b) using the erroneous horizontal kernel of length 12 pixels.

where $\mathbf{f}$ is the observed blurry image, $\mathbf{g}$ is the clear image to estimate; Φ is the fidelity term dependent on the nature of image noise and Ψ is the regularization term that enforces certain priors on de-blurred images. In the past, many image priors have been proposed for image deblurring. The Tikhonov regularization, $\Psi(\mathbf{g}) = \frac{1}{2}\|\Gamma\mathbf{g}\|_2^2$ with some difference operator Γ, is first proposed in [17] to enforce the smoothness of the underlying image. It is known that image edges of results from the Tikhonov method tend to be smoothed out. Thereafter, total variation (TV) and its variations (see e.g. [9], [18]–[21]) are developed to keep image edges sharper. TV-based regularizations are based on the ℓ_1 norm (or weighted ℓ_1 norm) of image gradients, i.e. $\Psi(\mathbf{g}) = \|\Gamma\mathbf{g}\|_1$ where Γ denote the first-order or higher-order difference operator. Also, some heavy-tailed statistical probabilistic constraints (e.g. [22]) are developed in recent years to regularize the de-blurred images. TV-based regularization tends to keep image edges sharper than Tikhonov regularization does. However, it is also observed that for nature images of complex structure, TV-based regularization does not preserve the image details very well on the regions of complex structures due to the stair-casing effects (see e.g. [23]).

Another promising regularization approach is based on the sparsity prior of images under certain transform domain, such as wavelet transform (see e.g. [24]). As most images are compressible signals, the sparsity priors assume that most coefficients of the image under these transforms are likely to be sparse, that is, most coefficients are zero or close to zero. Such sparsity priors are usually enforced via minimizing the ℓ_1 norm of transform coefficients of the image. For example, the wavelet tight frame transform is used in [25], [26] as the preferred transform to sparsify images. By using ℓ_1 norm of wavelet tight frame coefficients of images as the regularization strategy, impressive results are reported in [25], [26] for various image restoration tasks.

Besides Gaussian image noise, it is pointed out in Cho et al. [27] that some types of outlier, such as pixel saturation and non-Gaussian noise, will invalidate the convolution model such that the results deblurred by many existing methods have noticeable ringing artifacts. A new blur model is proposed in [27] is proposed to better deblur images by explicitly handling these types of outliers. Another problem is the so-called *boundary value problem* that also often causes ringing artifacts in the results if not appropriately handled. Boundary value problem in image deblurring is caused by the missing information of pixels outside the image boundary which is needed to produce the blurred image. Most existing strategy to solve this problem is to synthesize these unavailable pixels by

Fig. 2. Results in the presence of system error $\delta_{\mathcal{A}}$. The true blur kernel is linear motion blur kernel of length 20 pixels and orientation $45°$ to the horizonal axis counter-clockwise. The input blur kernel for deblurring is of length 20 pixels and orientation $50°$ to the horizontal axis counter-clockwise. (a) and (e): the original images, (b) and (f): the blurry images by true blur kernel, and (c) and (g): the blurry images by the input blur kernel, (d) and (h): the system error $\delta_{\mathcal{A}}\mathbf{g}$. Pixels values for (d) and (h) are magnified by ten times for better visual illustration.

extrapolating the available image data inside the image boundary. Various extrapolation schemes have been proposed in the past, including zero Dirichlet, periodic, Neumann (also called reflective or symmetric) boundary extension (see e.g. [28]). Usually, the periodic boundary extension is more suitable for methods working in frequency domain and Neumann boundary extension works better for regularization methods in spatial domain.

B. Motivation and the outline of our approach

As we stated in the previous discussion, the assumption that the blur kernel is free of error used in most existing methods often does not hold true in practice, especially in the case of motion blurring. As we observed in Fig. 1, the deblurring process is indeed very sensitive to the error in the matrix $\mathcal{A}$. One may take an alternating scheme attempting to correct kernel errors using the results obtained in the previous step, just as many blind deblurring methods do. However, the effectiveness of correcting kernel error by such an alternating iteration scheme largely relies on the accuracy the assumed kernel priors. Due to complex nature of real blurring processes, e.g., the spatially-variant nature of motion-blurring caused by camera shake, it remains a very challenging problem to have general priors on blur kernels that can accurately model most real data. Based on these observations, we propose to consider the following EIV (errors-in-variables) model for image deblurring:

$$\mathbf{f} = (\mathcal{A} - \delta_{\mathcal{A}})\mathbf{g} + \mathbf{n} \tag{5}$$

where $\mathbf{g}$ and $\mathbf{f}$ are the clear image and its blurred observation, $\mathcal{A}$ is the blurring matrix with model error δA and $\mathbf{n}$ is image noise.

The goal of this paper is to develop an efficient regularization method for solving (5) such that the de-blurred results are robust to both image noise $\mathbf{n}$ and model error $\delta_{\mathcal{A}}$. The basic idea of our proposed approach comes from the following rewritten form of (5):

$$\mathbf{f} = (\mathcal{A} - \delta_{\mathcal{A}})\mathbf{g} + \mathbf{n} = \mathcal{A}\mathbf{g} + \mathbf{n} - \delta_{\mathcal{A}}\mathbf{g}. \tag{6}$$

It is seen from (6) that to accurately estimate $\mathbf{g}$, we only need to know the residual term $\delta_{\mathcal{A}}\mathbf{g}$ instead of the perturbation matrix $\delta_{\mathcal{A}}$ itself. The perturbation matrix $\delta_{\mathcal{A}}$ is hard to estimate due to the lacking of information of
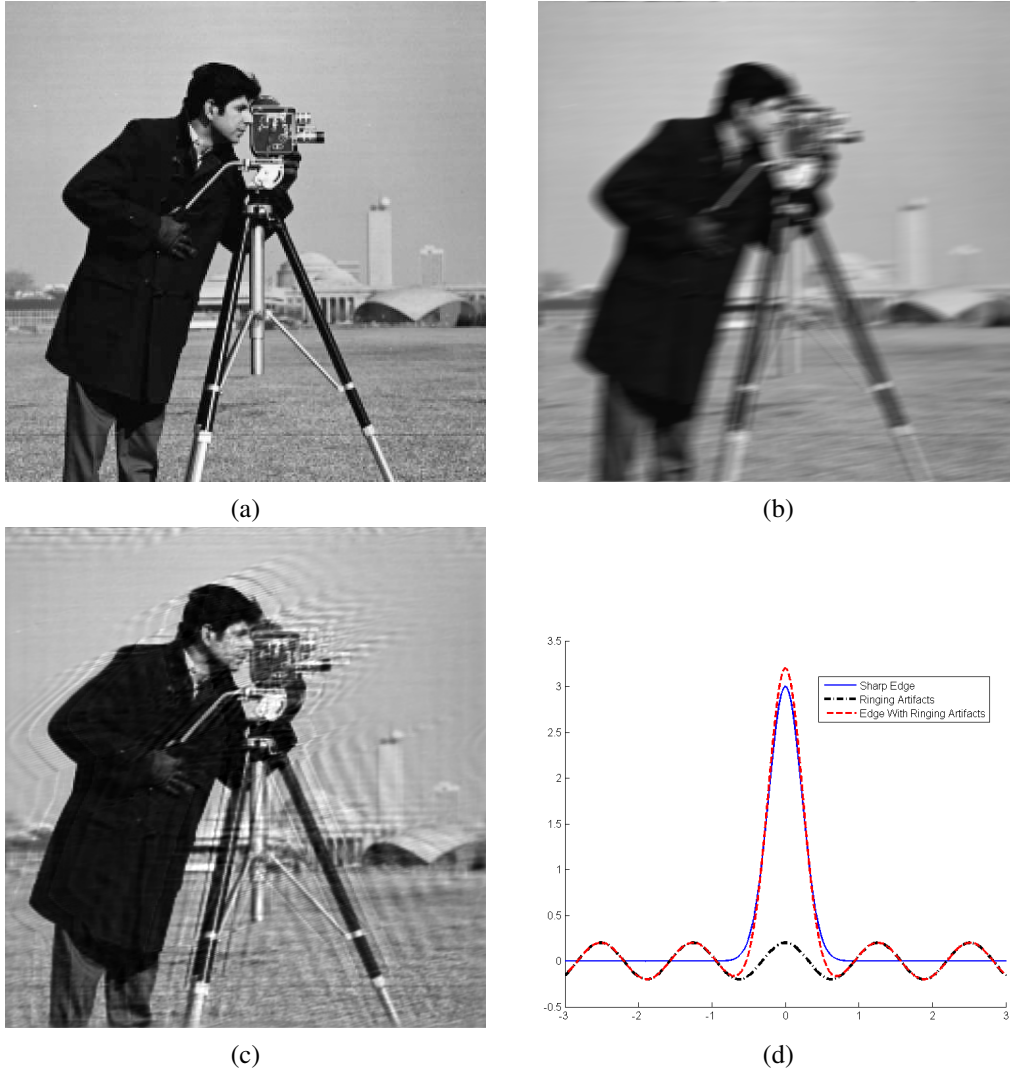
Fig. 3. Illustration of ringing effect caused by using erroneous kernel in RL method. (a): original image; (b): blurry image; (c): de-blurred result using RL method with an inaccurate kernel. (d): 1D illustration of the pattern of ringing artifacts along the normal direction of an image edge. The estimated edge, denoted as the red dashed line, is decomposed as an sharp edge and periodic function, denoted as the blue line and black dot-dash line respectively.

the blurring process. However, the estimation of the residual $\delta_{\mathcal{A}}\mathbf{g}$ is actually possible as there exist certain priors to constrain $\delta_{\mathcal{A}}\mathbf{g}$ well. As illustrated in Fig. 2, the residual term $\delta_{\mathcal{A}}\mathbf{g}$ tends to be sparse in the spatial domain. By enforcing the sparse prior of the residual $\delta_{\mathcal{A}}\mathbf{g}$, we can simultaneously estimate both the clear image $\mathbf{g}$ and the residual term $\delta_{\mathcal{A}}\mathbf{g}$ such that the error caused by $\delta_{\mathcal{A}}$ can be explicitly removed from the EIV model (6). Moreover, as illustrated in figure 3, the ringing artifacts caused by erroneous blur kernel usually show strong periodic patterns around the sharp edge, which can be modeled by the summation of the sharp edge and the pattern with strong periodicity. In our proposed regularization, we also explicitly separate these periodic patterns and sharp edges to further suppress the ringing artifacts in the results.

Furthermore, we propose a new approach for handling boundary value problem. Instead of explicitly extrapolating pixels outside the image boundary as most did, we propose to first estimate a clear image that includes all pixels involved in the generation of blurred image. The resulting estimation thus has a larger support than the given image does. Then the final result is obtained by cropping the estimated image to the same size as the given blurred image. By this technique, we avoid the possible error caused by the extrapolation which becomes noticeable when the blurring is significant.

The rest of the paper is organized as follows. In Section 2, we formalize the regularization strategy and explain the underlying motivation. In Section 3, we present the detailed numerical algorithm for solving the proposed

minimization problem. Section 4 is devoted to the experimental evaluation and discussions.

II. REGULARIZATION FORMULATION AND ANALYSIS

To overcome the sensitivity of image deblurring to image noise, certain image prior is needed to suppress the propagation of image noise when reversing the blurring process. Motivated by the impressive performance of the sparsity prior of images under tight wavelet frames in many image restoration tasks (e.g. [10], [29], [30]), we also use the ℓ_1 norm of wavelet tight frame coefficients of images as the regularization term to constrain clear images. Before we present the detailed minimization formula for robust image deblurring in the presence of model error in the blur kernel, we first give a brief introduction to wavelet tight frame.

A. Tight framelet system

In this section, we give a brief review on wavelet frame systems. For in-depth theoretical analysis and practical implementation, see for example [31], [32]. A wavelet frame system is a redundant system that generalizes the orthonormal wavelet basis (see [31] for more details). Wavelet tight frames have greater flexibility than orthonormal bases by sacrificing orthonormality and linear independence, while keeping the same efficient decomposition and reconstruction algorithms as orthonormal wavelet bases do. The filters used in wavelet frame systems have many attractive properties, not present in those used in orthonormal wavelet systems: *e.g.*, symmetry (anti-symmetry), smoothness,and shorter support. These nice properties make wavelet frame systems ideal for better representing images.

A MRA-based wavelet frame system is based on a single scaling function $\phi \in L^2(\mathbb{R})$ and several wavelet functions $\{\psi_1, \ldots, \psi_r\} \subset L^2(\mathbb{R})$ that satisfy the following refinable equation:

$$
\begin{aligned}
\phi(t) &= \sqrt{2} \sum_k h_0(k)\phi(2t-k); \\
\psi_\ell(t) &= \sqrt{2} \sum_k h_\ell(k)\phi(2t-k), \ell = 1, 2, \ldots, r.
\end{aligned}
$$

Let $\phi_k(t) = \phi(t-k)$ and $\psi_{k,j,\ell} = \psi_\ell(2^j t - k)$. Then for any square integrable function $f \in L^2(\mathbb{R})$, we have a multi-scale representation of f as the following

$$
f = \sum_{k=-\infty}^{\infty} c_k \phi_k(t) + \sum_{\ell=1}^{r} \sum_{j=0}^{\infty} \sum_{k=-\infty}^{\infty} d_{k,j,\ell} \psi_{k,j,\ell}, \tag{7}
$$

where $c_k = \int_{\mathbb{R}} f(t)\phi_k(t)dt$ and $d_{k,j,\ell} = \int_{\mathbb{R}} f(t)\psi_{k,j,\ell}(t)dt$. The equation above is called the *perfect reconstruction* property of wavelet tight frames. The coefficients $\{c_k\}$ and $\{d_{k,j,\ell}\}$ are called low-pass and high-pass wavelet coefficients. The wavelet coefficients can be efficiently calculated by a so-called cascade algorithm (see e.g. [24]). In this paper, we use the piece-wise linear wavelet frame developed in [31]:

$$
h_0 = \frac{1}{4}[1, 2, 1]; \ h_1 = \frac{\sqrt{2}}{4}[1, 0, -1]; \ h_2 = \frac{1}{4}[-1, 2, -1].
$$

See Fig. 4 for the corresponding scaling function ϕ, framelets ψ_1 and ψ_2.

In this paper, we follow the discrete implementation of 2D un-decimal multi-level framelet transform used in Cai et al [29]. Briefly, given the 2D tensor products of linear-piecewise framelet system associated with $h_k, k = 0, 1, 2$, let $\mathcal{H}$ denote the convolution operator with filter h, The multi-level decomposition operator up to L can be written as

$$
\mathcal{W} = \begin{bmatrix} \left(\prod_{\ell=0}^{L-1} \mathcal{H}_0^{(L-\ell)}\right)^\top ; \\ \left(\mathcal{H}_1^{(L)} \prod_{\ell=1}^{L-1} \mathcal{H}_0^{(L-\ell)}\right)^\top ; \left(\mathcal{H}_r^{(L)} \prod_{\ell=1}^{L-1} \mathcal{H}_0^{(L-\ell)}\right)^\top ; \\ \vdots \\ \left(\mathcal{H}_1^{(1)}\right)^\top ; \left(\mathcal{H}_r^{(1)}\right)^\top \end{bmatrix}^\top , \tag{8}
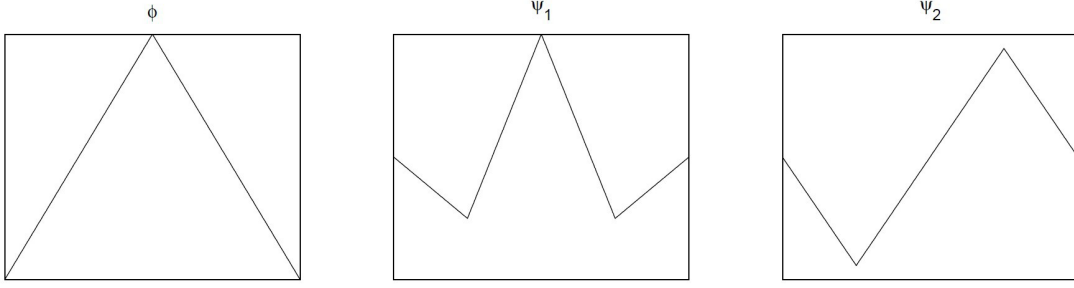$$

Fig. 4. Piecewise linear refinable scaling function and two corresponding framelets.

where $\mathcal{H}^{(i)}$ denote the convolution operators associated with the given filter H at the i-th level without down-sampling. For convenience of notation, we denote such a linear frame decomposition by a rectangular matrix $\mathcal{W}$ of size $m \times n$ with $m > n$. Thus, given any signal $\mathbf{f} \in \mathbb{R}^n$, the discrete version of (7) is expressed as the following

$$\mathbf{f} = \mathcal{W}^\top(\mathbf{c}) = \mathcal{W}^\top(\mathcal{W}\mathbf{f}),$$

where $\mathbf{c} \in \mathbb{R}^m$ is the frame coefficient vector of $\mathbf{f}$. It is noted that we have $\mathcal{W}^\top \mathcal{W} = \mathcal{I}_n$ but $\mathcal{W}\mathcal{W}^\top \neq \mathcal{I}_n$ unless the tight framelet system degenerates to an orthonormal wavelet system. We need to mention here that there exist fast algorithms for calculating $\mathcal{W}\mathbf{f}$ and $\mathcal{W}^\top\mathbf{c}$, which only involve the convolutions of images by a couple of filters. Interested readers are referred to [32] for more details.

B. Regularization model

Before presenting our proposed model in this section. We may first take a look at the system (5) in the absence of model error δ_A:

$$\mathbf{f} = \mathcal{A}\mathbf{g} + \mathbf{n},$$

There exist many robust methods for solving it. Our approach is built upon the framelet-based image deblurring method firstly proposed in [29], because of its impressive performance and rigorous mathematical treatment. The image deblurring method proposed in [29] is the so-called balanced approach for sparsity-based regularization, which recovers the clear image $\mathbf{g}$ via solving the following minimization:

$$\begin{cases} \mathbf{g}^* & := \mathcal{W}^\top \mathbf{c}^*; \\ \mathbf{c}^* & := \min_{\mathbf{c} \in \mathbb{R}^m} \frac{1}{2}\|\mathcal{A}\mathcal{W}^\top\mathbf{c} - \mathbf{f}\|_2^2 \\ & + \frac{\kappa}{2}\|(\mathcal{I}_m - \mathcal{W}\mathcal{W}^\top)\mathbf{c}\|_2^2 + \lambda\|\mathbf{c}\|_1 \end{cases} \tag{9}$$

where $0 \leq \kappa < \infty$ and λ is some regularization parameter, $\mathcal{I}_m$ denotes the identity matrix. $\mathbf{c}^*$ is the estimated framelet coefficient vector that will be used to synthesize the estimated clear image $\mathbf{g}^*$, via wavelet frame transform $\mathcal{W}^\top$. It is seen that the first term in the minimization is the ℓ_2 norm based data fidelity term that assume the existence of Gaussian white noise. The second term is the distance between the coefficient $\mathbf{c}$ and the range of $\mathcal{W}$, which is associated with the smoothness of the resulting image (see [32] for more details). The last term is ℓ_1 norm of framelet coefficient vector $\mathbf{c}$ that promotes the sparsity of the vector $\mathbf{c}$.

1) Minimization model in the presence of model error: When there exists the model error δ_A in the blur matrix $\mathcal{A}$, one additional error term $\delta_A\mathbf{g}$ appears in the system:

$$\mathbf{f} = (\mathcal{A} - \delta_A)\mathbf{g} + \mathbf{n} = \mathcal{A}\mathbf{g} - \delta_A\mathbf{g} + \mathbf{n}. \tag{10}$$

As we stated in the previous discussions, we propose to explicitly estimate the residual term $\delta_A\mathbf{g}$ via enforcing certain priors on $\delta_A\mathbf{g}$. The question remains how to constrain it. Notice that δ_A is the difference between two low-pass filters: the true blur kernel and the input blur kernel. Thus, the term $\delta_A\mathbf{g}$ is actually the response of the clear image $\mathbf{g}$ to some high-pass filters, which is likely to be sparse for nature images. See figure 2 for an illustration. Therefore, we propose to treat the residual term $\delta_A\mathbf{g}$ as an additional variable for estimation, which is done by regularizing it via a sparse constraint in the spatial domain.

Moreover, we observed that ring artifacts caused by the perturbation $\delta_{\mathcal{A}}$ generally have strong periodicity around the sharp edges. See figure 3 for an illustration of artifacts caused by kernel error when using the RL method . In other words, the results from erroneous kernel are the combination of sharp edges and periodic patterns. Recall that the signal with strong periodicity implies that most of its discrete cosine transform (DCT) coefficients are small, i.e., the DCT coefficient vector is sparse. Similar to the treatment of perturbation term $\delta_{\mathcal{A}}$, we also propose to further suppress the ringing artifacts caused by erroneous kernel by explicitly extracting these artifacts.

Thus, we proposed that the observed blurred image is composed by two parts: one is the composite of the true image and the artifacts blurred by the true kernel; the other is the response of clear image in some high-pass filter channel. This leads to the following minimization model for deblurring in the presence of model error $\delta_{\mathcal{A}}$:

$$\begin{cases} \mathbf{g}^* & := \mathcal{W}^T \mathbf{c}^*; \\ \{\mathbf{c}^*, \mathbf{h}^*, \mathbf{u}^*\} & := \operatorname{argmin}_{\mathbf{c}, \mathbf{h}, \mathbf{u}} \Phi(\mathbf{c}, \mathbf{h}, \mathbf{u}) \\ & \quad + \lambda_1 \|\mathbf{c}\|_1 + \lambda_2 \|\mathbf{h}\|_1 + \lambda_3 \|\mathbf{u}\|_1 \end{cases} \tag{11}$$

with

$$\begin{aligned} \Phi(\mathbf{c}, \mathbf{h}, \mathbf{u}) &= \tfrac{1}{2} \|\mathcal{A}(\mathcal{W}^\top \mathbf{c} + \mathcal{C}^\top \mathbf{h}) + \mathbf{u} - \mathbf{f}\|_2^2 \\ &\quad + \tfrac{\kappa}{2} \|(\mathcal{I}_m - \mathcal{W}\mathcal{W}^T) \mathbf{c}\|_2^2, \end{aligned} \tag{12}$$

where $\mathcal{C}$ denotes the DCT operator, and $\mathbf{c} \in \mathbb{R}^m, \mathbf{h} \in \mathbb{R}^n, \mathbf{u} \in \mathbb{R}^n$ denote three variables that represent the wavelet frame coefficients of clear image, the DCT coefficients of ringing artifacts and the residual $\delta_{\mathcal{A}}\mathbf{g}$ respectively. The minimization model (11)–(12) essentially decomposes the blurred image into three components regularized by different sparsity-based priors:

1) clear image $\mathbf{g}^* = \mathcal{W}^T \mathbf{c}^*$, which has a nearly sparse representation in wavelet frame domain;
2) ringing artifacts $\mathbf{h}^*$, whose DCT coefficient vector is nearly sparse;
3) system residual $\mathbf{u}$, which is sparse in the spatial domain.

It is easy to see that the minimization model (11) is convex and there exists a very efficient numerical method for solving (11) detailed in Section 3.

2) Modified minimization model (11) with boundary value problem handling: The system (5) will not be exact in the neighborhood of image boundaries, as the pixels involved in the generation of pixels along the boundary of image $\mathbf{f}$ are missing in the system. This is the so-called boundary value problem in image deblurring. Instead of extrapolating these pixels using pixels inside the boundary as most methods do, we propose a new approach that can be naturally incorporated into the model (11). The basic idea is to first estimate all pixels involved in the generation of the observed blurry image, then crop it to the same size as the observed image. Let Ω denote the set of all pixels inside the image boundary and let Ω^c denote denote the set of pixels outside of the image boundary but involved in the blurring process. Now let the variable $\mathbf{c} \in \mathbb{R}^{m'}$ denote the wavelet tight frame coefficient vector that generates an image $\mathcal{W}^\top \mathbf{c}$ with the support $\Omega \cup \Omega^c$. Then, to incorporate the new boundary handling strategy, we only need to modify the minimization model (11) as the following

$$\begin{aligned} \Phi(\mathbf{c}, \mathbf{h}, \mathbf{u}) &= \tfrac{1}{2} \|[\mathcal{A}(\mathcal{W}^\top \mathbf{c} + \mathcal{C}^\top \mathbf{h})]_\Omega + \mathbf{u} - \mathbf{f}\|_2^2 \\ &\quad + \tfrac{\kappa}{2} \|(\mathcal{I}_{m'} - \mathcal{W}\mathcal{W}^\top) \mathbf{c}\|_2^2, \end{aligned} \tag{13}$$

where $\mathbf{c} \in \mathbb{R}^{m'}, \mathbf{h} \in \mathbb{R}^{n'}$, and $\mathbf{u} \in \mathbb{R}^n$. And the result is defined as $\mathbf{g}^* = (\mathcal{W}^\top \mathbf{c}^*)|_\Omega$. Notice that the difference between models (11) and (13) lies on which image region to work on. By defining a projection operator $\mathcal{P}_\Omega$ which sets the values of pixels in Ω^c to 0 and unchanged otherwise, the model (13) can be written as

$$\begin{aligned} \Phi(\mathbf{c}, \mathbf{h}, \mathbf{u}) &= \tfrac{1}{2} \|\mathcal{P}_\Omega(\mathcal{A}(\mathcal{W}^\top \mathbf{c} + \mathcal{C}^\top \mathbf{h})) + \mathbf{u} - \mathbf{f}\|_2^2 \\ &\quad + \tfrac{\kappa}{2} \|(\mathcal{I}_{m'} - \mathcal{W}\mathcal{W}^\top) \mathbf{c}\|_2^2, \end{aligned} \tag{14}$$

The advantage of this approach over the existing explicit boundary extension is that it avoids extrapolating the pixel values outside of the boundary, which becomes quite unreliable when the blurring is significant.

C. Numerical algorithm

In this section, we give a detailed description of the efficient numerical solver for the minimization (14) derived in last section. The minimization (14) is a convex but has non-differentiable terms. In recent years, there have been great progresses on how to solve this type of ℓ_1 related minimization problems. In particular, the so-called *Accelerated*

Proximal Gradient (APG) method has been used by [33], [34] for solving similar ℓ_1-regularized minimization problems arising in various image/signal processing applications. Its fast convergence rate is not only mathematically proved but also demonstrated in various image restoration tasks (see [34]). Thus, the APG method is chosen in our implementation as the numerical solver for the minimization problem (14). For the completeness, we first give a brief introduction of the generic APG algorithm. Interesting readers are referred to [33], [34] for more details.

The APG algorithm is designed for solving the following convex optimization model

$$\min_{x \in \mathbb{R}^n} F(x) + G(x) \tag{15}$$

where the term F is convex, continuously differentiable and its gradient ∇F is Lipschitz continuous on $\mathbb{R}^n$, i.e.

$$\|\nabla F(x) - \nabla F(y)\|_2 \leq L\|x - y\|_2, \quad \forall\, x, y \in \mathbb{R}^n$$

for some constant $L > 0$, and the term G is convex but not necessarily differentiable. The general APG method for solving (15) is outlined in Algorithm 1. It is seen that the only non-trivial step is the second step in (16) which also requires solve an optimization sub-problem. Fortunately, when $G(x) = \lambda\|x\|_1$, the solution to such an sub-problem can be easily computed with a simple soft-thresholding operator. More specifically, the soft-thresholding operator $\mathcal{T}_\lambda$ is defined as the following

$$\mathcal{T}_\lambda : x = [x_1, x_2, ..., x_n] \mapsto [t_{\lambda_1}(x_1), t_{\lambda_2}(x_2), ..., t_{\lambda_n}(x_n)]$$

with $t_{\lambda_i}(x_i) = \mathrm{sgn}(x_i)\max\{0, |x_i| - \lambda_i\}$. Then, for the second step in (16), we have

$$x_{k+1} = \mathcal{T}_{\lambda/L}\big(\beta_k - \frac{1}{L}\nabla F(\beta_k)\big).$$

It is shown in [33] that Algorithm 1 only need $O(1/\sqrt{\epsilon})$ iterations to yield a solution with the ϵ-optimality to (15).

Theorem 2.1:[33] Let the sequence $\{x_k\}$ be generated by Algorithm 1 and let x^* be any minimizer of (15). Then for any $k \geq 1$

$$\Big|[F(x_k) + G(x_k)] - [F(x^*) + G(x^*)]\Big| \leq \frac{2L\|x_0 - x^*\|_2^2}{(k+1)^2}.$$

Algorithm 1 Numerical algorithm for solving (15)

(i) Set initial guesses $x_0 = x_{-1} \in \mathbb{R}^n$ and set $t_0 = 1, t_{-1} = 0$.

(ii) For $k = 0, 1, \ldots$, perform the following iterations until convergence

$$\begin{cases} \beta_k & := x_k + \frac{t_{k-1}-1}{t_k}(x_k - x_{k-1}); \\ x_{k+1} & := \mathrm{argmin}_{x \in \mathbb{R}^n} G(x) \\ & \quad + \frac{L}{2}\Big\|x - \big(\beta_k - \frac{1}{L}\nabla F(\beta_k)\big)\Big\|^2; \\ t_{k+1} & := \frac{1+\sqrt{1+4t_k^2}}{2}. \end{cases} \tag{16}$$

The general APG method can be applied to solve our proposed model (14) with little modifications. For the minimization (14), we have

$$\begin{aligned} F(\mathbf{c}, \mathbf{h}, \mathbf{u}) &= \tfrac{1}{2}\|\mathcal{P}_\Omega \mathcal{A}(\mathcal{W}^T\mathbf{c} + \mathcal{C}^\top\mathbf{h}) + \mathbf{u} - \mathbf{f}\|_2^2 \\ &\quad + \tfrac{\kappa}{2}\|(\mathcal{I}_{m'} - \mathcal{W}\mathcal{W}^T)\mathbf{c}\|_2^2. \end{aligned}$$

It is easy to see that F is a differentiable convex function with L-Lipschtiz gradient. Its gradients with respect to $\mathbf{c}, \mathbf{h}, \mathbf{u}$ are as the following

$$\begin{cases} \nabla_{\mathbf{c}} F(\mathbf{c}, \mathbf{h}, \mathbf{u}) &= \mathcal{W}\mathcal{A}^T\mathcal{P}_\Omega^T\big[\mathcal{P}_\Omega \mathcal{A}(\mathcal{W}^T\mathbf{c} + \mathcal{C}^\top\mathbf{h}) + \mathbf{u} - \mathbf{f}\big] \\ &\quad + \kappa(\mathcal{I}_{m'} - \mathcal{W}\mathcal{W}^T)\mathbf{c}; \\ \nabla_{\mathbf{h}} F(\mathbf{c}, \mathbf{h}, \mathbf{u}) &= \mathcal{C}\mathcal{A}^T\mathcal{P}_\Omega^T\big[\mathcal{P}_\Omega \mathcal{A}(\mathcal{W}^T\mathbf{c} + \mathcal{C}^\top\mathbf{h}) + \mathbf{u} - \mathbf{f}\big]; \\ \nabla_{\mathbf{u}} F(\mathbf{c}, \mathbf{h}, \mathbf{u}) &= \mathcal{P}_\Omega \mathcal{A}(\mathcal{W}^T\mathbf{c} + \mathcal{C}^\top\mathbf{h}) + \mathbf{u} - \mathbf{f}. \end{cases}$$
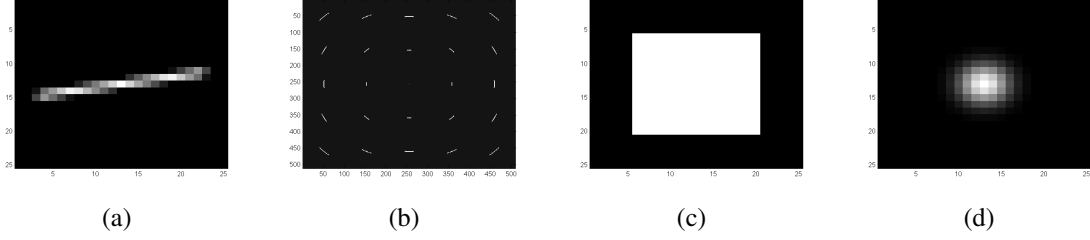
Fig. 5. Four sample kernels tested in the experiments. (a): linear motion blur kernel of length 20 pixels and of slop $10°$ to the horizontal axis counter-clockwise; (b): illustration of piece-wise blurring process caused by camera rotation of $10°$; (c): box blur kernel of size 15×15 pixels, (d): Gaussian blur kernel with $\sigma = 3$.

Notice that the model (11) is a special case of (14) by setting the projection operator $\mathcal{P}_\Omega$ the identity matrix. Thus, we only give the detailed description of the numerical algorithm for solving (14); see Algorithm 2. In our implementation, L is set as 4, κ is set as 1. The initial guess $\mathbf{c}_0$ are the coefficients of given blurry image under framelet decomposition, $\mathbf{u}_0$ and $\mathbf{h}_0$ are all set as the zero vector $\mathbf{0}$.

Algorithm 2 the APG method for solving (14)

(i) Set initial guesses $\mathbf{c}_0 = \mathbf{c}_{-1} \in \mathbb{R}^{m'}, \mathbf{h}_0 = \mathbf{h}_{-1} \in \mathbb{R}^{n'}, \mathbf{u}_0 = \mathbf{u}_{-1} \in \mathbb{R}^{n'}$ and set $t_0 = 1, t_{-1} = 0$.

(ii) For $k = 0, 1, \ldots$, perform the following iterations until $\|\mathcal{W}(\mathbf{c}_{k+1} - \mathbf{c}_k)\|_2 \leq \epsilon$:

$$
\begin{cases}
\beta_k^c & := \mathbf{c}_k + \frac{t_{k-1}-1}{t_k}(\mathbf{c}_k - \mathbf{c}_{k-1}); \\
\beta_k^h & := \mathbf{h}_k + \frac{t_{k-1}-1}{t_k}(\mathbf{h}_k - \mathbf{h}_{k-1}); \\
\beta_k^u & := \mathbf{u}_k + \frac{t_{k-1}-1}{t_k}(\mathbf{u}_k - \mathbf{u}_{k-1}); \\
\mathbf{g}_k^c & := \beta_k^c - \nabla_{\mathbf{c}} F(\beta_k^c, \beta_k^h, \beta_k^u)/L; \\
\mathbf{g}_k^h & := \beta_k^h - \nabla_{\mathbf{h}} F(\beta_k^c, \beta_k^h, \beta_k^u)/L; \\
\mathbf{g}_k^u & := \beta_k^u - \nabla_{\mathbf{u}} F(\beta_k^c, \beta_k^h, \beta_k^u)/L; \\
\mathbf{c}_{k+1} & := \mathcal{T}_{\lambda_1/L}(\mathbf{g}_k^c); \\
\mathbf{h}_{k+1} & := \mathcal{T}_{\lambda_2/L}(\mathbf{g}_k^h); \\
\mathbf{u}_{k+1} & := \mathcal{T}_{\lambda_3/L}(\mathbf{g}_k^u); \\
t_{k+1} & := \frac{1+\sqrt{1+4t_k^2}}{2}.
\end{cases}
\tag{17}
$$

III. NUMERICAL EXPERIMENTS AND ANALYSIS

Through all the experiments, the parameters λ_2, λ_3 are set as $5\lambda_1$ and $2\lambda_1$ respectively in our implementation. The value of λ_1 is dependent on the image noise level. In our implementation, it is set as $5e^{-4}$ when there is little noise and is set as the value close to the standard deviation of image noise otherwise. The Matlab (Version 7.11) implementation of the deblurring algorithms are performed on an PC with an Intel Core 2 CPU of 2.4GHz and with 4GB RAM. The average time assumption for an image of size 256×256 pixels is around 20 seconds.

A. Simulated images

In the first part of the experiments, the proposed method is tested on synthesized degraded images. The test images are blurred by the given blur kernels followed by adding additional Gaussian white noise. Four representative types of blur kernels are tested in the experiments: a) translational motion blur kernel (spatially invariant), (b) blurring matrix from rotational motion blurring (spatially varying), (c) box blur kernel and (d) Gaussian blur kernel. Both proposed models, model (11) with Neumann boundary extension and model (14) with proposed boundary value problem handling technique, are compared against three existing representative deblurring methods: the Richardson-Lucy method [35], the TV based regularization method [36] and the wavelet frame based regularization method [25]. Besides the visual comparison of the results, the PSNR measurement is also used to quantitatively evaluate

blur type	true kernel	input kernel
linear motion blurring	length: 20 pixels orientation: $10°$	length: 20 pixels orientation: $20°$
spatially varying blurring	motion blurring by image rotation of $10°$	piecewise linear blur kernel
box-type blurring	size: 15×15	size 17×17
Gaussian blurring	$\sigma = 2$	$\sigma = 3$

TABLE I

THE TRUE BLUR KERNELS OF BLURRED IMAGES AND THE ERRONEOUS INPUT OF THE DEBLURRING ALGORITHMS

the quality of the restored results. Recall that given a signal $\mathbf{x}$, the *peak signal to noise ratio* (PSNR) of its estimate is defined as

$$\mathrm{PSNR}(\widehat{\mathbf{x}}, \mathbf{x}) = 10 \log_{10} \frac{255^2}{\frac{1}{mn} \sum_{i=1}^{m} \sum_{j=1}^{n} (\widehat{\mathbf{x}}_{ij} - \mathbf{x}_{ij})^2},$$

where (m, n) is the size of the image, $\mathbf{x}_{ij}$ is the intensity value at the pixel location (i, j), and $\widehat{\mathbf{x}}_{ij}$ corresponds to the intensity value of the restored image at the location (i, j).

In the experiments, four sample images shown in Fig. 6 (a) – Fig. 9 (a) are first blurred by four sample blur kernels shown in Fig. 5 respectively, and then added by additional Gaussian white noise with different standard deviation (std). The inaccurate blur kernels used as the input of the deblurring methods are listed in Table I. It is noted that the blurring process caused by in-plane image rotation varies everywhere in the image. And we use a piece-wise uniform blurring process to model it, that is, partition the blurred image into multiple sub-regions and assume each sub-region is blurred by a linear motion blur kernel.

The PSNR values of the results from all five methods are summarized in Table II and Table III. It is seen that there are noticeable advantages of the model (11) and (13) over other methods in terms of PSNR values. The benefits using the proposed boundary problem handing are also demonstrated in this experiment, as the model (14) outperformed (11) in most cases. The improvement on PSNR value is also consistent with the improvement on visual quality. See Fig. 6 – Fig. 9 for an visual inspection of some sample results with respect to both noise-free and noisy cases. It is clear that the results from the two proposed methods have the least artifacts among all methods. Overall, the model (14) is the best performer in this experiment, in terms of both PSNR values and visual quality.

In the remains of this section, we would like to show how the performance of the proposed method scales with the degree of kernel error by a simple experiment. The experiment is run on the image "cameraman" blurred by a linear motion kernel with length 20 pixels and orientation $10°$ to the horizontal axis counter-clockwise. The blurred image is deblurred by the proposed model (14) using different erroneous kernels. The erroneous kernels are also linear motion kernels of length 20 pixels but with different orientations: $15°$, $20°$, $30°$ and $40°$. In other words, the orientation errors of the input kernels are $5°$, $10°$, $20°$ and $30°$ respectively. See Fig. (10) for the visualization of the corresponding results. It is not surprising to see that the performance of the proposed method decreases when the error increases. When the estimation error becomes very significant, e.g., more than $20°$ error in the orientation of linear motion blur kernel, the results are smoothed out. To correct the results in the presence of very significant kernel error, some additional module has to be incorporated into the method to correct the estimation of the blur kernel.

B. Real images

In the second experiment, the proposed methods are applied on real motion-blurred images and the results are compared with the following three methods: RL method ([35]), TV regularization method ([36]) and wavelet frame regularization method ([25]). Since the model (14) with the proposed boundary value problem handling technique shows better performance than the model (11) with Neumann boundary extension. We only included the results from (14). During the experiment, all motion-blur kernels are first inferred using the two-phase blind motion deblurring method recently proposed by [37]. Then the inferred motion-blur kernels are used as the input of all non-blind methods for comparison. Due to the complexity of real motion-blur kernels and the spatially varying nature of practical motion blurring, the error in blurring matrix is unavoidable, which can be seen from the results from the blind motion deblurring method ([37]).
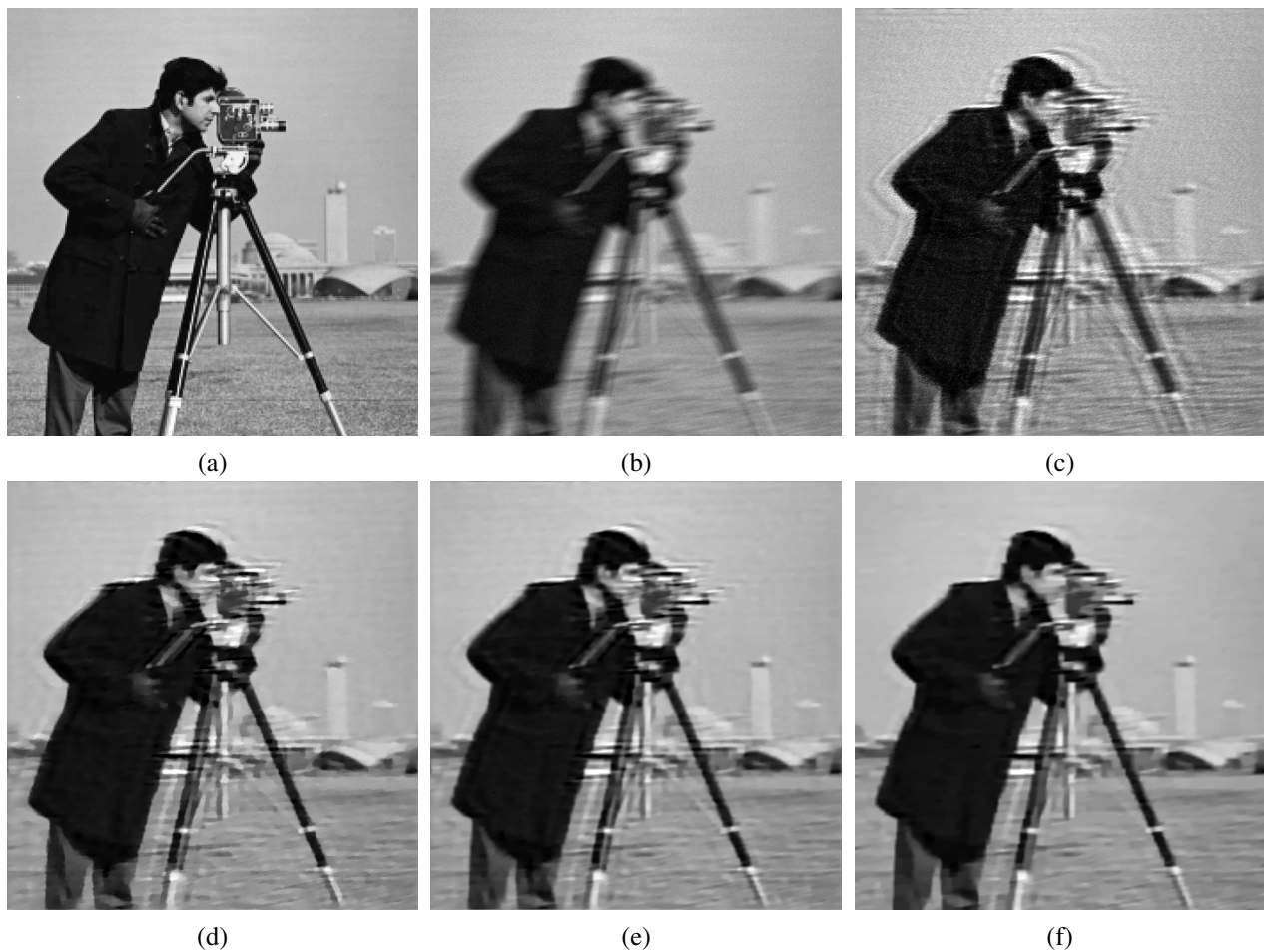
Fig. 6. Results of removing linear motion blur from image "cameraman" in the presence of Gaussian white noise with std = 5. (a): the ground truth image; (b): the blurred and noisy image (c)–(f): the results of RL method ([35]), TV method ([36]), wavelet frame method ([25]) and the proposed model (14), respectively.
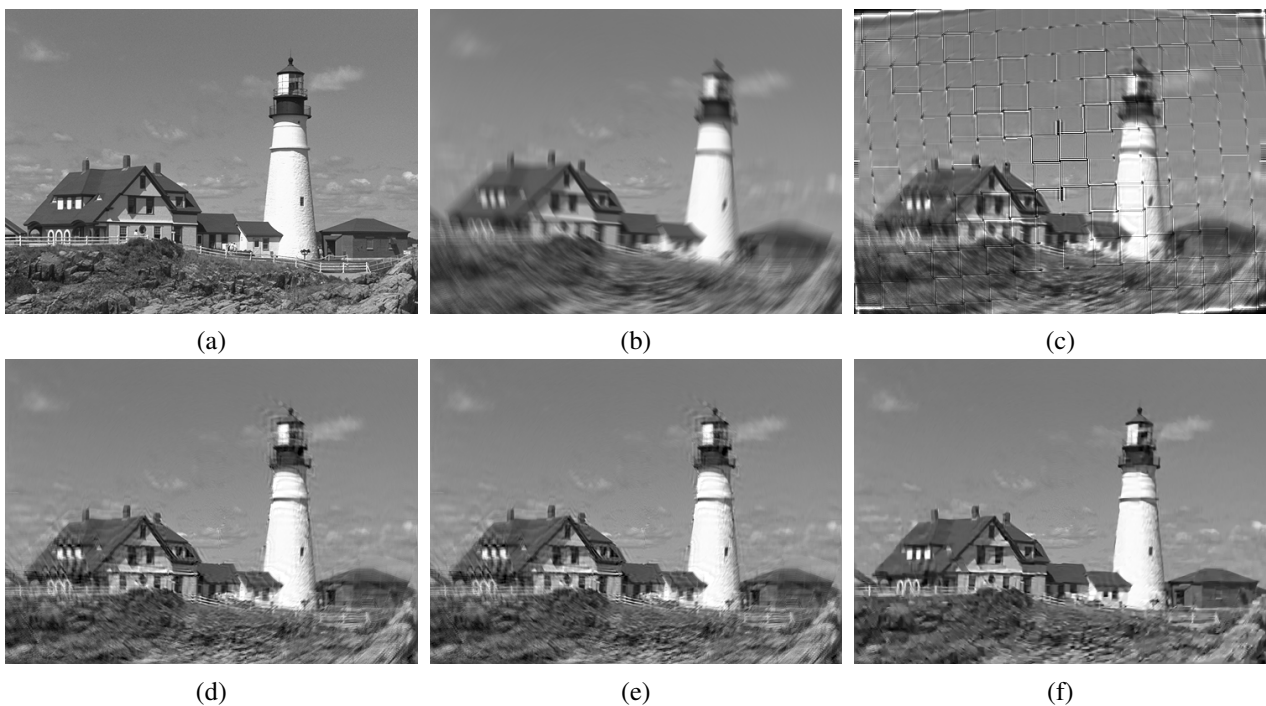

Fig. 7. Results of removing rotational motion blurring from noise-free image "towergray". (a): the ground truth image; (b): the input blurry image; (c)–(f): the results of the RL method [35], the TV method [36], wavelet frame method [25] and the proposed model 14, respectively.

Translational Motion Blur (Spatially Invariant)						
	Noise std	[35]	[36]	[25]	(11)	(14)
Cameraman	0	22.75	23.94	23.93	24.38	**24.48**
	5	21.75	23.81	23.82	23.96	**24.06**
Lena	0	24.98	26.27	26.08	26.40	**26.81**
	5	23.53	25.82	25.81	26.05	**26.23**
Towergray	0	17.55	21.99	22.10	22.99	**23.05**
	5	14.00	21.83	21.83	22.95	**23.00**
Logo	0	15.73	16.70	17.65	18.29	**18.30**
	5	15.60	16.59	17.62	18.02	**18.02**
Rotational Motion Blur (Spatially Variant)						
	Noise std	[35]	[36]	[25]	(11)	(14)
Cameraman	0	16.17	26.54	26.85	27.43	**28.03**
	5	15.95	26.26	26.51	26.77	**27.04**
Lena	0	18.06	28.18	28.37	29.01	**29.74**
	5	17.74	27.72	28.13	28.34	**28.68**
Towergray	0	18.43	25.35	25.32	25.68	**26.21**
	5	18.09	23.02	24.85	25.01	**25.13**
Logo	0	16.44	28.67	28.65	**29.23**	29.22
	5	16.41	25.33	28.25	28.68	**28.70**

TABLE II

PSNR VALUES OF THE RESULTS BY FIVE METHODS W.R.T. TWO TYPE OF MOTION BLURRING: SPATIALLY INVARIANT MOTION BLURRING AND SPATIALLY VARYING MOTION BLURRING

Out-of-focus Blurring (Box kernel)						
	Noise std	[35]	[36]	[25]	(11)	(13)
Cameraman	0	23.33	25.66	25.72	26.31	**26.55**
	5	22.91	25.01	24.95	25.06	**25.08**
Lena	0	25.24	27.32	27.13	27.62	**27.77**
	5	24.63	26.41	26.37	26.39	**26.71**
Towergray	0	23.03	23.40	23.43	23.63	**23.83**
	5	22.41	23.19	23.27	23.47	**23.52**
Logo	0	16.51	18.65	19.21	**19.52**	19.50
	5	15.90	18.04	18.36	18.64	**18.66**
Optical Blurring (Gaussian Kernel)						
	Noise std	[35]	[36]	[25]	(11)	(13)
Cameraman	0	23.72	25.31	25.56	26.65	**26.97**
	5	23.24	25.29	25.51	26.33	**26.44**
Lena	0	26.57	27.42	27.91	28.49	**29.15**
	5	25.64	27.39	27.83	28.37	**28.92**
Towergray	0	23.50	24.02	24.16	24.62	**24.63**
	5	23.03	23.98	24.14	24.52	**24.54**
Logo	0	14.60	18.28	21.55	**22.25**	22.24
	5	14.53	18.28	21.51	22.13	**22.18**

TABLE III

PSNR VALUES OF THE RESULTS BY FIVE METHODS W.R.T. BOX BLUR KERNEL AND GAUSSIAN BLUR KERNEL

Two types of motion-blurred images are tested. The first is two motion-blurred images caused by camera shake from Levin et al. [11]. In [11], both the blurry images and the corresponding true clear images are provided, which are obtained by specific hardware configurations. Both images tested in the experiment are of size 255×255 and blurred by motion-blur kernel of size ranging from 13×13 to 27×27. The motion blur process occurring on these two images is mostly a spatially invariant motion blur process, perturbed by a small amount of spatially varying blurring process. The results are shown in Fig. 11, it is seen that there are noticeable artifacts in the results from the blind deblurring method. Switching to other two existing non-blind deblurring methods does not improve the results either. On the contrary, the results from the proposed approach (14) has the least artifacts among all. In other words, the results from blind deblurring methods can be further improved by our proposed robust non-blind deblurring model (14), owing to its built-in mechanism of handling model error in the blur matrices. Also, the

Fig. 8. Results of removing box blurring from noise-free image "lena". (a): the ground truth image, (b): the input blurry image; (c)–(f): the results of the RL method [35], the TV method [36], the wavelet frame method [25] and the proposed model 14, respectively.

	Blind deblurring [37]	TV [36]	Wavelet [25]	Model (14)
"Crown"	24.86	24.74	22.23	**26.58**
"Children"	25.28	24.16	22.83	**26.04**

TABLE IV
PSNR VALUES OF THE RESULTS SHOWN IN FIGURE 11

visual improvement from our proposed model is consistent with the improvement of PSNR value; see Table IV for the comparison of PSNR values of the results from all compared methods.

In practice, due to the varying depth of the scene, it is also often seen that motion blurring happened on the images are spatially varing. For this type of images, we still use the same two-stage blind deblurring methods [37] to estimate a global motion kernel by assuming the motion blurring is spatially invariant. Then this motion-blur kernel is used to de-blur the images using existing non-blind deblurring methods and our proposed method. The tested real images are either from [38] or taken by a Canon EOS 550D DSLR camera. The results are shown in Fig. 12 and Fig. 13. Clearly, our approach yielded the results with least artifacts and it showed that our method indeed is robust to possible modeling error in blurring matrices. All kernels of tested images inferred by the two-stage method [37] are shown in Fig. 14.

IV. CONCLUSIONS

In this paper, a new regularization method is developed for non-blind image deblurring which is robust to error in kernel, noise image and boundary value problem. The resulting minimization problem is convex and can be efficiently solved by the APG method with fast convergence. The proposed method can either be used to deblur images when only blur kernel of low quality is available, or can be used to deblur images blurred by complex

Fig. 9. Results of removing Gaussian blurring from image "logo" in the presence of image noise with std = 5. (a): the ground truth image; (b): the input blurry and noisy image; (c)–(f): the results of the RL method [35], the TV method [36], the wavelet frame method [25] and the proposed model (14), respectively.

blurring processes such as spatially varying motion blurring. In future, we would like investigate how to incorporate such a framework to solve the blind motion-blurring problem when there are fast moving objects in the scene.

REFERENCES

[1] N. Joshi, R. Szeliski, and D. Kriegman, "PSF estimation using sharp edge prediction," in *CVPR*, 2008. 1, 2

[2] A. Levin, Y. Weiss, F. Durand, and W. T. Freeman., "Understanding and evaluating blind deconvolution algorithms." MIT-CSAIL-TR-2009-014, Tech. Rep., 2009. 1

[3] Y. Tai, H. Du, M. Brown, and S. Lin, "Correction of spatially varying image and video blur using a hybrid camera," *IEEE PAMI*, 2009. 1, 2

[4] M. Ben-Ezra and S. K. Nayar, "Motion-based motion deblurring," *IEEE Trans. PAMI*, vol. 26, no. 6, pp. 689–698, 2004. 2

[5] R. Raskar, A. Agrawal, and J. Tumblin, "Coded exposure photography: Motion deblurring via fluttered shutter," in *SIGGRAPH*, vol. 25, 2006, pp. 795–804. 2

[6] Y. Tai, H. Du, M. Brown, and S. Lin, "Image/video deblurring using a hybrid camera," in *CVPR*, 2008. 2

[7] A. Rav-Acha and S. Peleg, "Two motion blurred images are better than one," *Patt. Recog. Lett.*, vol. 26, pp. 311–317, 2005. 2

[8] L. Yuan, J. Sun, L. Quan, and H. Shum, "Blurred/non-blurred image alignment using an image sequence," in *SIGGRAPH*, 2007. 2

[9] Q. Shan, J. Jia, and A. Agarwala, "High-quality motion deblurring from a single image," in *SIGGRAPH*, 2008. 2, 3

[10] J.-F. Cai, H. Ji, C. Liu, and Z. Shen, "Blind motion deblurring from a single image using sparse approximation," in *CVPR*, 2009. 2, 6

[11] A. Levin, F. Durang, Y. Fredo, and W. T. Freeman, "Understanding and evaluating blind deconvolution algorithms," in *CVPR*, 2009. 2, 13, 17

[12] A. Levin, P. Sand, T. S. Cho, F. Durand, and W. T. Freeman, "Motion invariant photography," *ACM Trans. Graphics*, 2008. 2

[13] A. J. Jain, *Fundamentals of digital image processing*. Prentice-Hall, 1989. 2

[14] W. H. Richardson, "Bayesian-based iterative method of image restoration," *Journal of the Optical Society of America*, vol. 62, no. 1, p. 55?9., 1972. 2

[15] L. B. Lucy, "An iterative technique for the rectification of observed distributions," *Astronomical Journal*, vol. 79, no. 6, pp. 745–754, 1974. 2
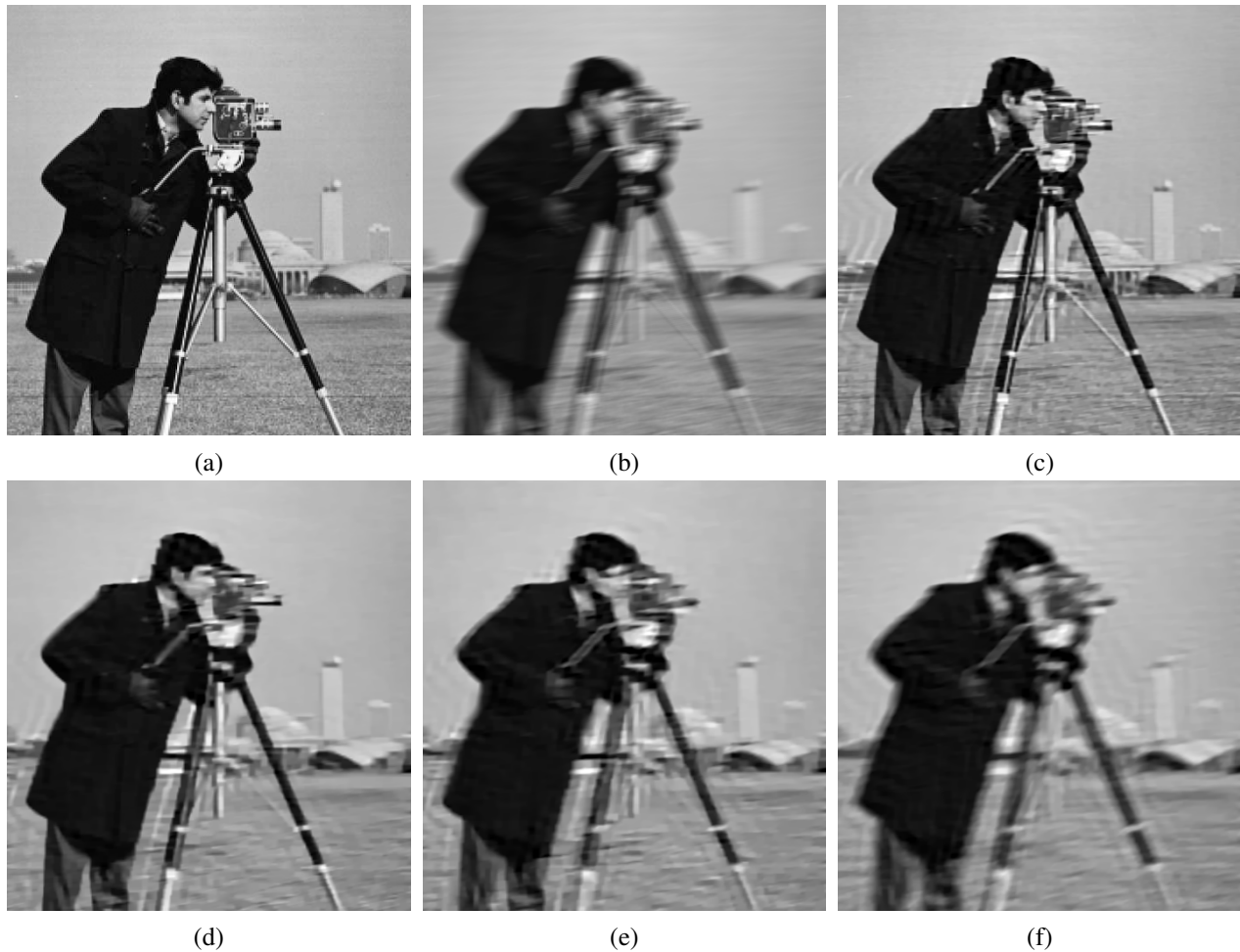
Fig. 10. Results of removing motion blurring from image "cameraman". (a): the ground truth image, (b): the input blurry image blurred by linear motion kernel with length 20 pixels and orientation $10°$ to the horizontal axis counter-clockwise. (c)–(f): the results of the proposed model (14) using errorneous blur kernels with orientation error $5°$, $10°$, $20°$ and $30°$ respectively.

[16] Y. Tai, P. Tan, M. Brown, "Richardson-Lucy deblurring for scenes under projective motion path," *IEEE PAMI*, Vol. 33, no. 8, pp. 1603-1618, 2011. 2

[17] A. N. Tikhonov, V. Y. Arsenin, and F. John, *Solution of ill-posed problems*. VH Washinton D.C., 1977. 3

[18] T. F. Chan and C. K. Wong, "Total variation blind deconvolution," *IEEE Tran. Image Processing*, vol. 7, no. 3, pp. 370–375, 1998. 3

[19] T. Chan, A. Marquina, and P. Mulet, "High-order total variation-based image restoration," *SIAM J. Sci. Comput.*, vol. 22, pp. 503–516, 2000. 3

[20] N. Dey, L. Blanc-Fraud, C. Zimmer, Z. Kam, P. Roux, J. Olivo-Marin, and J. Zerubia, "A deconvolution method for confocal microscopy with total variation regularization," in *IEEE International Symposium on Biomedical Imaging: Nano to Macro*, 2004. 3

[21] T. F. Chan and J. Shen, *Image Processing and Analysis: Variational, PDE, wavelet, and stochastic methods*. SIAM, 2005. 3

[22] R. Fergus, B. Singh, A. Hertzmann, S. T. Roweis, and W. T. Freeman, "Removing camera shake from a single photograph," in *SIGGRAPH*, vol. 25, 2006, pp. 783–794. 3

[23] M. Nikolova, "Local strong homogeneity of a regularized estimator," *SIAM J. Appl. Math.*, vol. 61, pp. 633–658, 2000. 3

[24] S. Mallat, *A Wavelet Tour of Signal Processing*. Academic Press, 1999. 3, 6

[25] J. Cai and Z. Shen, "Framelet based deconvolution," *J. Comp. Math*, 2008. 3, 10, 11, 12, 13, 14, 15, 17, 18, 19

[26] J.-F. Cai, S. Osher, and Z. Shen, "Linearized bregman iterations for frame-based image deblurring," *SIAM Journal on Imaging Sciences*, pp. 226–252, 2009. 3

[27] S. Cho, J. Wang, and S. Lee, "Handling outliers in non-blind image deconvolution," in *Proc. IEEE International Conference on Computer Vision (ICCV 2011)*, 2011, pp. 1–8. 3

[28] R. Chan, M. Ng, and W. Tang, "A fast algorithm for deblurring models with neumann boundary conditions," *SIAM J. Sci. Comput.*, vol. 21, pp. 851–866, 1999. 4

[29] J.-F. Cai, R. Chan, and Z. Shen, "A framelet-based image inpainting algorithm," *Appl. Comput. Harmon. Anal.*, vol. 24, pp. 131–149, 2008. 6, 7

[30] J.-F. Cai, S. Osher, and Z. Shen, "Split bregman methods and frame based image restoration," *Multiscale Modeling and Simulation: A SIAM Interdisciplinary Journal*, vol. 8, no. 2, pp. 337–369, 2009. 6

| full image | region | full image | region |

Fig. 11. Results of two real images from [11]. the first row: true clear images; the second row: blurred images; the third row: the results from blind deblurring method [37]; the 4th to 6th row: the results from the TV regularization algorithm [36], the wavelet frame regularization method [25] and the proposed model (14) respectively.

| full image | region | full image | region |

Fig. 12. Results of two real images from [38]. The first row: blurred images; the second row: the results from blind deblurring method [37]; the third to 5th row: the results from the TV regularization algorithm [36], the wavelet frame regularization method [25] and the proposed model (14) respectively.

[31] I. Daubechies, B. Han, A. Ron, and Z. Shen, "Framelets: MRA-based constructions of wavelet frames," *Appl. Comput. Harmon. Anal.*, vol. 14, pp. 1–46, 2003. 6

[32] Z. Shen, "Wavelet frames and image restorations," in *Proceedings of the International Congress of Mathematicians*, vol. 4, 2010, pp. 2834–2863. 6, 7

[33] A. Beck and M. Teboulle, "A fast iterative shrinkage-thresholding algorithm for linear inverse problems," *SIAM Journal on Imaging Sciences*, vol. 2, no. 1, pp. 183–202, 2009. 9

[34] Z. Shen, K. Toh, and S. Yun, "An accelerated proximal gradient algorithm for frame based image restorations via the balanced approach," *SIAM Journal on Imaging Sciences*, 20xx. 9

[35] W. H. Richardson, "Bayesian-based iterative method of image restoration," *Journal of the Optical Society of America (1917- 1983), 62:55?9, 1972.*, vol. 62, pp. 55–59, 1972. 10, 11, 12, 13, 14, 15

[36] C. Wu and X. Tai, "Augmented Lagrangian method, dual methods, and split Bregman iteration for ROF, vectorial TV, and high order models," *SIAM Journal on Imaging Sciences*, vol. 3, p. 300, 2010. 10, 11, 12, 13, 14, 15, 17, 18, 19

[37] L. Xu and J. Jia, "Two-phase kernel estimation for robust motion deblurring," *Computer Vision–ECCV 2010*, pp. 157–170, 2010. 11, 14, 17, 18, 19, 20

Fig. 13. Results of two real images taken by a Canon EOS 550D camera. The first row: blurred images; the second row: the results from blind deblurring method [37]; the third to 5th row: the results from the TV regularization algorithm [36], the wavelet frame regularization method [25] and the proposed model (14) respectively.
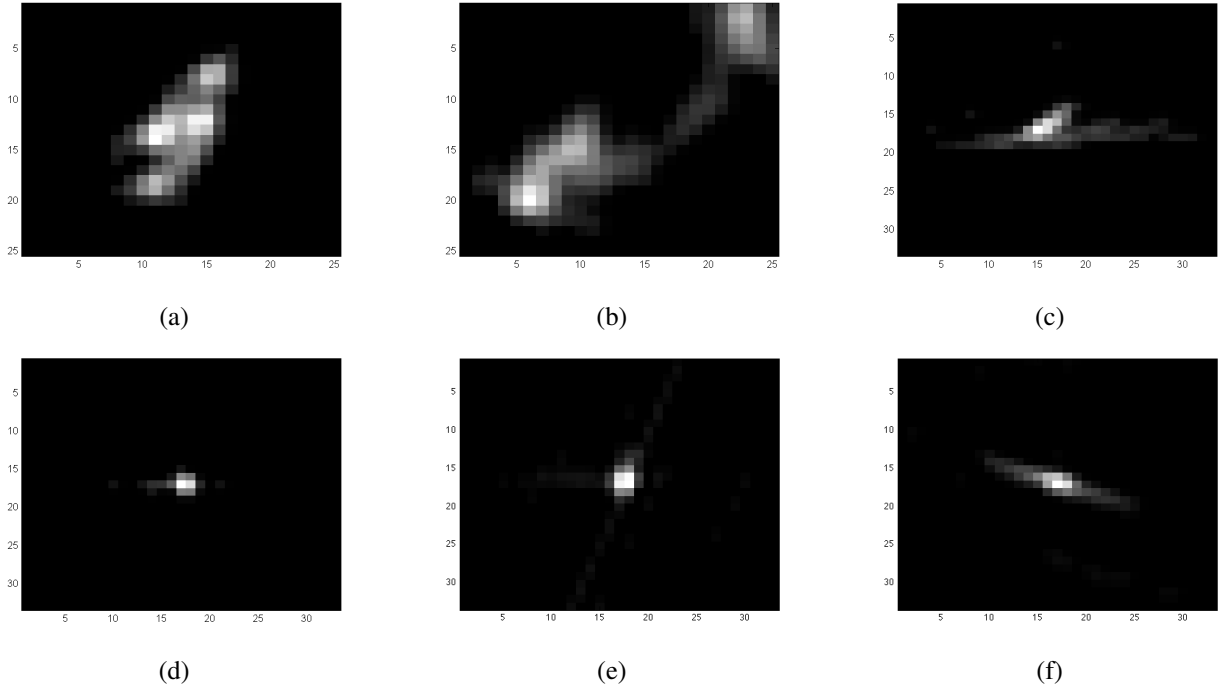
Fig. 14. Kernels estimated by the approach of [37]. (a) and (b) are the estimated kernels for the two blurry images shown in Fig. 11; (c) and (d) are the estimated kernels for the two blurry images shown in Fig. 12; (e) and (f) are the estimated kernels for the two blurry images shown in Fig. 13.

[38] A. Gupta, N. J. N., C. L. Zitnick, and M. Cohen, "Single image deblurring using motion density functions," in *ECCV*, 2010. 14, 18

Hui Ji received the BSc degree from Nanjing University in China, the MSc degree in mathematics from National University of Singapore in Singapore and the PhD degree in computer science from University of Maryland, College Park, USA. Since 2006, he has been an assistant professor in Department of Mathematics at National University of Singapore in Singapore. His research interests are in human and computer vision, image and video processing, computational harmonic analysis and optimization.
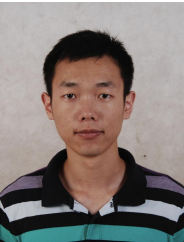
Kang Wang received the BSc degree in Mathematics from Shanghai Jiao Tong University, China in 2009. He is currently a PhD candidate in the Department of Mathematics at National University of Singapore in Singapore. His research interests are in image processing, wavelet, compressive sensing, and related problems.